

## THERMAL MANAGEMENT AND PHASE CHANGE HEAT TRANSFER CHARACTERISTICS OF $\text{LiFePO}_4$ BATTERIES BY COOLING PHASE CHANGE MATERIALS

by

**Yaoting WANG<sup>a</sup>, Tong MENG<sup>a</sup>, and Wenxiao CHU<sup>b,\*</sup>**

<sup>a</sup> Xi'an Institute of Space Radio Technology, Xi'an, Shaanxi, China

<sup>b</sup> Key Laboratory of Thermal-Fluid Science and Engineering, Ministry of Education,  
Xi'an Jiaotong University, Xi'an, Shaanxi, China

Original scientific paper  
<https://doi.org/10.2298/TSCI210724338W>

*The cycle life and thermal safety of lithium-iron-phosphate ( $\text{LiFePO}_4$ ) batteries are important factors restricting the popularization of new energy vehicles. The study aims to prevent battery overheating, prolong the cycle life of power batteries and improve their thermal safety by discussing the heat production of  $\text{LiFePO}_4$  batteries to solve the problem of temperature rise in the natural-convection environment and cut the energy consumption in the liquid cooling system. A numerical simulation and experiment are employed to study the heat production characteristics of  $\text{LiFePO}_4$  batteries and the heat transfer characteristics of the system, with its PCM and coupling PCM of paraffin and expanded graphite), channel liquid, and micro-channel PCM coupling cooled to control the temperature of the batteries. The results show that the temperature goes higher with the discharge rate during discharge. Since it has large internal component values,  $\text{LiFePO}_4$  produces more heat at the beginning and end of discharge. When the battery pack is discharged at 1C and 2C rates, the mass-flow rates are  $1.8 \cdot 10^{-3}$  kg/s and  $3.6 \cdot 10^{-3}$  kg/s, the temperature can be controlled at most 40 °C, and the temperature difference less than 3 °C, respectively. Paraffin is composed of expanded graphite, and the thermal conductivity of the composite heat storage PCM (phase change heat storage materials) is 24 times of that of pure paraffin. Therefore, cooling the active liquid and coupled PCM can improve the cooling efficiency and has a good effect on solving the problem of temperature rise and energy consumption reduction. The research provides a reference for the thermal energy management of  $\text{LiFePO}_4$  batteries, providing a method of cooling PCM of  $\text{LiFePO}_4$  batteries.*

Key words: *thermal management of  $\text{LiFePO}_4$  batteries, material cooling,  $\text{LiFePO}_4$  batteries, phase change heat transfer*

### Introduction

As problems like energy crisis and environmental pollution are increasingly prominent, the energy conservation, emission reduction, and sustainable development of the automobile industry with large global carbon emissions attract more and more attention [1, 2]. Developing new energy vehicles with low energy consumption and emissions can realize the sustainable development of the automobile industry [3]. Energy electric (EV) vehicle uses electric energy as driving energy. Compared with fuel vehicles, it attracts much attention for its advantages of being friendlier to environments and low energy consumption [4]. At present, the

\* Corresponding author, e-mail: wxchu84@xjtu.edu.cn

common EV on the market are mainly divided into hybrid, pure electric, and fuel-cell vehicles [5]. As people pay more and more attention environmental protection, many countries in the world provide corresponding support for the spread of new energy EV [6].

The safety of batteries is an important factor limiting the popularity of new energy vehicles [7]. The  $\text{LiFePO}_4$  batteries are one of the three core parts of new energy vehicles. It is very important to make it run stably in a safe environment. However, its performance is closely related to its temperature [8]. Therefore, it requires designing a thermal management system that can apply to EV. Power battery is another core component of new energy vehicles. The safety and driving range of new energy vehicles largely depend on the characteristics of power batteries [9]. The power batteries on the market are mainly lead-acid,  $\text{LiFePO}_4$ , Ni MH batteries, and fuel cells [10]. Since the invention of the lead-acid battery in 1859, the technology has been relatively mature after years of development, with good stability and low cost [11-13]. At present, the main onboard batteries of traditional fuel vehicles are still lead-acid batteries [14]. However, due to the low energy density of lead-acid batteries and the environmental pollution caused by its development process, the development of lead-acid batteries as a power battery in new energy vehicles is seriously affected. Therefore, it is not appropriate to use the lead-acid battery in pure EV [15]. Although the environmental pollution of Ni MH battery is less than that of lead-acid battery, there are also many shortcomings in the performance of the battery, such as scattered energy distribution and high rate of self-discharging, which also limit its development in EV [16]. Compared with lead-acid and Ni MH batteries, the fuel cell has a high energy density [17], and it has no pollution the environment, which will be the development direction of a vehicle power cell in the future [18, 19]. However, at present, the fuel cell has the problems of high development cost and long cycle, and it will take a long time to be widely used. Since it has the advantages of a high discharge platform, good cycle performance, and non-memory effect, a  $\text{LiFePO}_4$  battery is the best choice for new energy electric vehicles [20].

Researchers have done a lot of research on the thermal energy management of lithium-iron-sulfate batteries. Zhou *et al.* [21] carried out a series of experimental studies on the thermal failure characteristics of fully charged  $\text{LiFePO}_4$  batteries by copper elastic battery calorimetry. It provides total external heat (16 kJ) for the battery at different heating power (20-200 W). The battery temperature, exhaust start time, mass loss, and internal heat are measured and analyzed. The results show that with the increase of heating power, the start time of exhaust and thermal runaway decreases exponentially. The calorific value of the battery under different heating powers is within 10.38 kJ-15.07 kW. The maximum temperature and calorific value of the battery do not increase monotonously with the heating power but reach the maximum at 100 W. The experimental data provide a reference for the safety design of battery components and the prevention of thermal failure propagation. Cheng *et al.* [22] conducted overheating abuse experiments on prismatic lithium-ion battery components. The cellular behavior and characterization during thermal runaway propagation are studied, including gas emission, flame emission, flame combustion, sound characteristics, and heat transfer. In the experiment, the central battery is heated on both sides until the electrode temperature exceeds 300 °C, and the heat is out of control for about 43 minutes and spreads from the central to both sides in the module. All 12 batteries are burned. The results show that the first three uncontrolled batteries first emit gas and then emit sounds with similar amplitude, frequency, and energy, about 200 seconds earlier than flame injection. Then, the characteristic of the internal short circuit is that the temperature rate region is 1.0 K per second and the time is more than 20 seconds. The experimental results provide in-depth understanding, thermal runaway warning, and evaluation methods for module security design. Cui *et al.* [23] studied battery health problems and energy management problems which

brought great challenges to hybrid electric buses. The proposed optimal energy management methods while prolonging the battery life. Based on the battery cycle test, a semi-empirical aging model of the  $\text{LiFePO}_4$  battery is established and identified by data fitting. However, the research on the thermal energy management of lithium-iron-sulfate batteries is not profound enough.

Based on the thermal safety of power cells, the heat production characteristics of  $\text{LiFePO}_4$  batteries are studied by a numerical simulation and an experiment. The heat transfer characteristics of the system are studied for the heat management system of PCM cooling, channel-liquid cooling, and coupled PCM cooling, respectively. In the process of establishing the heat production model of  $\text{LiFePO}_4$  batteries, the previous research mainly uses the form of a fixed heat source. After the internal resistance of the cell is obtained by the hybrid pulse method, the real-time update of the heat source is realized by programming user defined function (UDF) in FLUENT. This method has a certain guiding significance for improving the accuracy of the battery heat-production model.

## Methods of thermal energy management and heat transfer characteristics of $\text{LiFePO}_4$ batteries

### *Framework and principle of $\text{LiFePO}_4$ batteries*

The framework of  $\text{LiFePO}_4$  batteries is composed of cathode fluid, cathode material, diaphragm, anode material, and negative fluid, which are alternated and stacked with each other, as shown in fig 1.

The cathode material of  $\text{LiFePO}_4$  batteries is a lithium intercalation compound, and the capacity of  $\text{LiFePO}_4$  batteries is largely determined by the electrochemical characteristics and lattice characteristics of cathode material. The  $\text{LiFePO}_4$  battery with lithium-iron-sulfate cathode material is often used as a power battery because of its excellent charge-discharge characteristics at a high rate and long cycle life. The role of anode materials in  $\text{LiFePO}_4$  batteries is to provide a stable storage environment for lithium ions. At present, the most common anode materials used in  $\text{LiFePO}_4$  batteries are carbon-based materials [24]. The electrolyte is distributed on both sides of the diaphragm, which is the medium for lithium-ion transport [25]. The diaphragm exists between the cathode and anode materials, and it is used to block the cathode and anode materials to ensure that the free electrons inside the battery are blocked and cannot pass through, thereby ensuring the safe operation of the battery. The cathode and negative fluids connect the cathode and anode materials of the battery and conduct electricity.

Although the  $\text{LiFePO}_4$  battery has many advantages, its performance is greatly affected by temperature. Therefore, the heat production characteristics of square  $\text{LiFePO}_4$  batteries are analyzed, and the thermal management mode of the battery system is studied [26]. The cathode material of  $\text{LiFePO}_4$  batteries is connected with that of the battery through an aluminum foil fluid, and the negative material is graphite, which is attached to the negative fluid. The cathode and anode materials are separated by a diaphragm in the middle. During charging,  $\text{Li}^+$  enters the electrolyte from ferric sulfate, passes through the diaphragm, enters the surface of negative graphite crystal, and finally embeds into graphite. At the same time, electrons flow into the anode material through the circuit of cathode fluid, and finally into the anode material of the graphite, making the charge balanced [27]. The chemical reaction equation of the charging process:

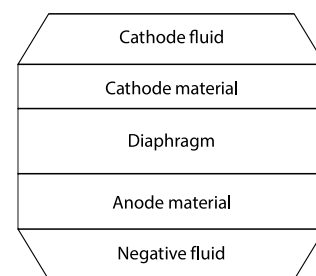
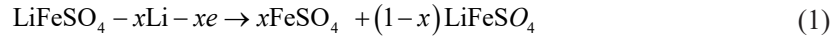
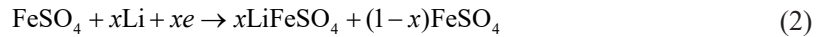


**Figure 1. Internal structure of  $\text{LiFePO}_4$  batteries**



The chemical reaction equation in the discharge process can be expressed:



#### Heat production characteristics of lithium battery

Chemical reaction heat,  $Q_r$ , polarization heat,  $Q_s$ , ohmic heat,  $Q_j$ , and negative reaction heat,  $Q_p$ , are the main heat sources of LiFePO<sub>4</sub> batteries during charging and discharging. The total heat production,  $Q$ :

$$Q = Q_r + Q_s + Q_j + Q_p \quad (3)$$

where  $Q_r$  is the heat of a chemical reaction. During charging, the reaction is endthermic [28]. The  $Q_r$  is negative, and  $Q_r$  is positive. The calculation equation:

$$Q_r = \frac{nmQ_{rn}I}{MF} \quad (4)$$

where  $n$  is the number of batteries,  $m$  – the mass of electrode,  $Q_{rn}$  – the algebraic sum of the heat produced by the cathode and anode materials,  $I$  – the charging and discharging current,  $M$  – the molar mass,  $F$  – the faraday constant,  $Q_s$  – the polarization heat, and  $Q_j$  – the ohmic heat: [29]:

$$Q_j = I^2 R_j \quad (5)$$

where  $I$  is the charge-discharge current and  $R_j$  – the ohmic internal resistance.

The energy conservation differential equation in the unsteady heat conduction can be established by taking any microelement in the battery as the research object:

$$\rho c \frac{\partial T}{\partial \tau} = \frac{\partial}{\partial x} \left( \lambda_x \frac{\partial T}{\partial x} \right) + \frac{\partial}{\partial y} \left( \lambda_y \frac{\partial T}{\partial y} \right) + \frac{\partial}{\partial z} \left( \lambda_z \frac{\partial T}{\partial z} \right) + qr \quad (6)$$

where  $\rho c(\partial T/\partial \tau)$  is the thermodynamic increment of the cell, and

$$\frac{\partial}{\partial x} \left( \lambda_x \frac{\partial T}{\partial x} \right) + \frac{\partial}{\partial y} \left( \lambda_y \frac{\partial T}{\partial y} \right) + \frac{\partial}{\partial z} \left( \lambda_z \frac{\partial T}{\partial z} \right)$$

is the increased energy of the cell in unit time through the heat conduction of the interface. The  $T$  is the temperature of the microelement,  $c$  – the specific heat capacity,  $\rho$  – the density,  $qr$  – the heat production rate,  $\lambda_x$ ,  $\lambda_y$ , and  $\lambda_z$  are the thermal conductivity in the direction  $x$ ,  $y$ ,  $z$ .

The interior of LiFePO<sub>4</sub> batteries is composed of a variety of materials. The calculation equation of thermal conductivity:

$$\lambda_x = \frac{x}{\sum \frac{\Delta x_i}{\lambda_i}} \quad (7)$$

where  $x$  is the thickness of the battery,  $\Delta x_i$  – the thickness of each material, and  $\lambda_i$  – the thermal conductivity of the materials.

The density  $\rho$  and specific heat capacity  $c$  of Li-ion batteries are generally calculated by weighted average:

$$\rho = \frac{\sum m_i}{\sum v_i} \quad (8)$$

$$c = \frac{1}{m_c} \sum c_i m_i \quad (9)$$

where  $m_i$ ,  $v_i$ ,  $c_i$  are the mass, volume, and specific heat of each component and  $m_c$  is the total mass.

Since the actual heat production of LiFePO<sub>4</sub> batteries is complex, it needs to make corresponding hypotheses on the heat production process of LiFePO<sub>4</sub> batteries. Based on these hypotheses, the battery heat production model is expressed:

$$q_r = \frac{Q}{V} = \frac{I}{V} \left( E - U - T \frac{dE}{dT} \right) \quad (10)$$

where  $V$  is the volume,  $I$  – the current,  $E$  – the open circuit voltage,  $U$  – the working voltage, and  $dT$  – the temperature coefficient, with the value of  $-0.4$  mV/K. The equation is simplified:

$$q_r = \frac{1}{V} \left( I^2 R - IT \frac{dE}{dT} \right) \quad (11)$$

#### *Heat transfer characteristics of lithium battery*

The ohmic internal resistance and that of the polarization in the state of charge (SOC) can be calculated:

$$R_j = \frac{U_2 - U_1}{I} \quad (12)$$

$$R_p = \frac{U_3 - U_2}{I} \quad (13)$$

In the test of internal resistance, the SOC value of the battery is adjusted to the corresponding value, and the battery is kept for a while, and then the battery is pulsed discharge to obtain the internal resistance of the battery under different SOC conditions. The heat production in different SOC states can be calculated by eq. (11). Subsequently, the calculated results are fitted by a five-order polynomial to obtain the characteristic curve of the heat production rate per unit volume of the battery with time. The fitting equation of the heating rate and time of the battery during discharge at different rates:

$$q_r = A_1 \times t^5 + A_2 \times t^4 + A_3 \times t^3 + A_4 \times t^2 + A_5 \times t + A_6 \quad (14)$$

The values of  $A_1 \sim A_6$  are different at different discharge rates.

The simulation analysis of the heat production model is carried out and compared with the results of the experiment. Based on the research results, the heat production source of the battery is realized by UDF programming in the software.

According to the experimental environment, the boundary conditions for solving the temperature distribution are:

$$T(r, \phi, z) = T_0 \quad (15)$$

$$\bar{q} = h(T - T_\infty) \quad (16)$$

$\bar{q}$  is the heat flux,  $h$  – the heat transfer coefficient,  $T$  – the surface temperature,  $T_0$  – the battery initial temperature, and  $T_\infty$  – the ambient temperature.

*Heat transfer characteristics of LiFePO<sub>4</sub> batteries based on cooling PCM*

The governing equations related to fluid and heat transfer include continuity, momentum conservation, and energy conservation. Since the fluid is incompressible, its continuity equation:

$$\nabla \vec{v} = 0 \quad (17)$$

The momentum conservation equation:

$$\frac{\partial \vec{v}}{\partial t} + \vec{v} \nabla \vec{v} = f - \frac{1}{\rho_w} \nabla P + \vec{v} \nabla^2 \vec{v} \quad (18)$$

The energy conservation equation:

$$\frac{\partial}{\partial t} (\rho_w c_{p,w} T_w) + \nabla (\rho_w c_{p,w} \vec{v} T_w) = \nabla (k_w \nabla T_w) \quad (19)$$

$$\frac{\partial}{\partial t} (\rho_c c_{p,c} T_c) = \nabla (k_c \nabla T_c) \quad (20)$$

$\rho_w$ ,  $c_{p,w}$ ,  $K_w$ ,  $T_w$ , and  $\vec{v}$  are the density, specific heat capacity, thermal conductivity, temperature, and velocity vector of water,  $\rho_c$ ,  $c_{p,c}$ ,  $K_c$ ,  $T_c$  – the density, specific heat capacity, thermal conductivity, and temperature of the cooling plate, respectively, and  $f$  – the mass force for fluid.

### Results of thermal energy management and heat transfer characteristics of LiFePO<sub>4</sub> batteries

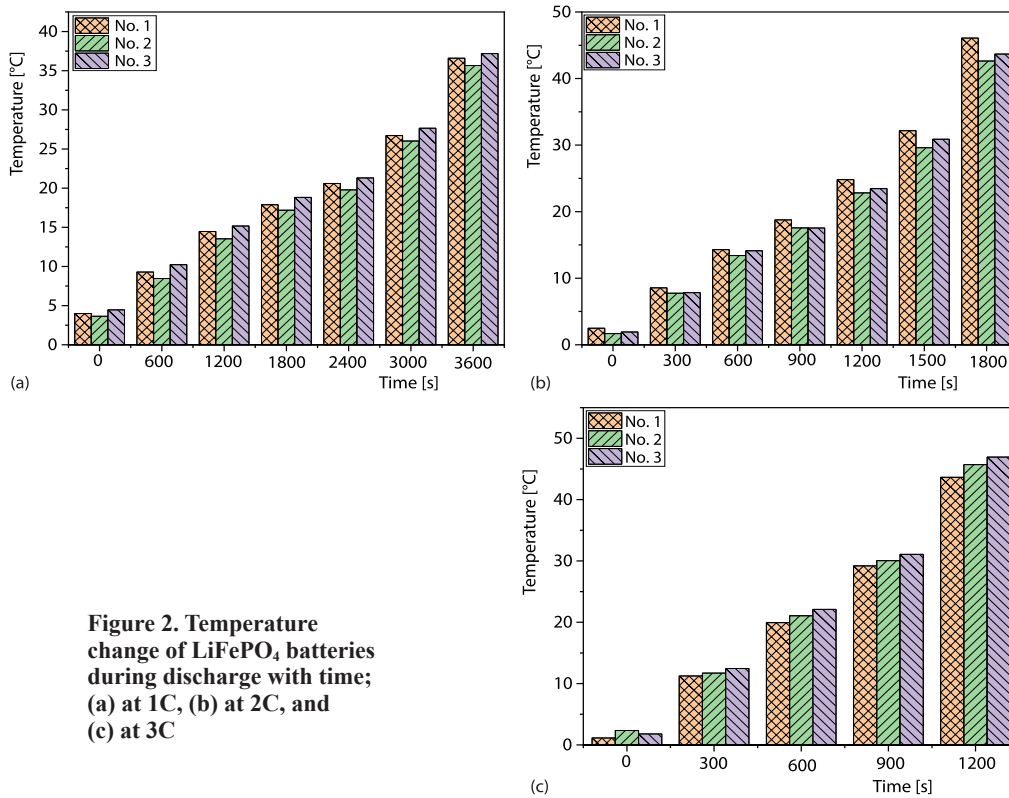
#### *Experimental results of heat production of single cell*

The discharge temperature of LiFePO<sub>4</sub> batteries varies with time during discharge, as shown in fig. 2.

Figure 2 shows that the temperature increases with that of the discharge rate. This is because the current flowing through the battery at a high discharge rate is high, thereby increasing the heat production. At the same time, the accumulation of heat in a short time cannot be released in time, and the temperature of the battery is positively correlated with the discharge rate. Besides, the temperature of LiFePO<sub>4</sub> batteries increases rapidly in the initial and the later stage of discharge, because the heat production of LiFePO<sub>4</sub> batteries in these two-stages is larger.

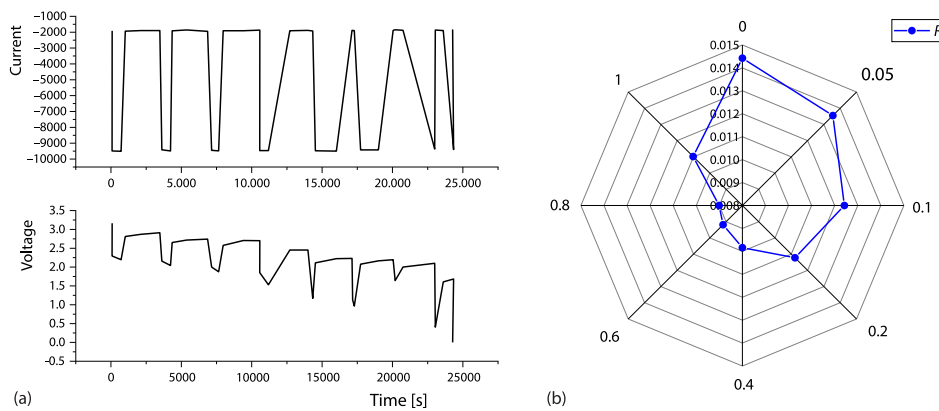
The hybrid pulse power characteristic (HPPC) test is carried out on the battery. The voltage curve obtained in the test can be used to verify the reliability and accuracy of the battery model under variable current. The test data under different states of charge can be obtained by multiple standing, and the specific test process refers to the U. S. Freedom CAR Power Assisted Hybrid Electric Vehicle Battery Testing Manual, which is divided into 11 steps:

- Step 1. Stand for 10 minutes.
- Step 2. Be filled with 1C constant current constant voltage.
- Step 3. Stand still for one hour.
- Step 4. The 1C constant current discharge 10%.
- Step 5. Stand still for one hour.
- Step 6. The 3C constant current discharge 10 seconds.
- Step 7. Stand for 30 seconds.
- Step 8. The 2.25C constant current charging 10 seconds.
- Step 9. Stand for 30 seconds.
- Step 10. Repeat Steps 4-9 ten times.
- Step 11. The 1C constant current discharging to cut-off voltage.



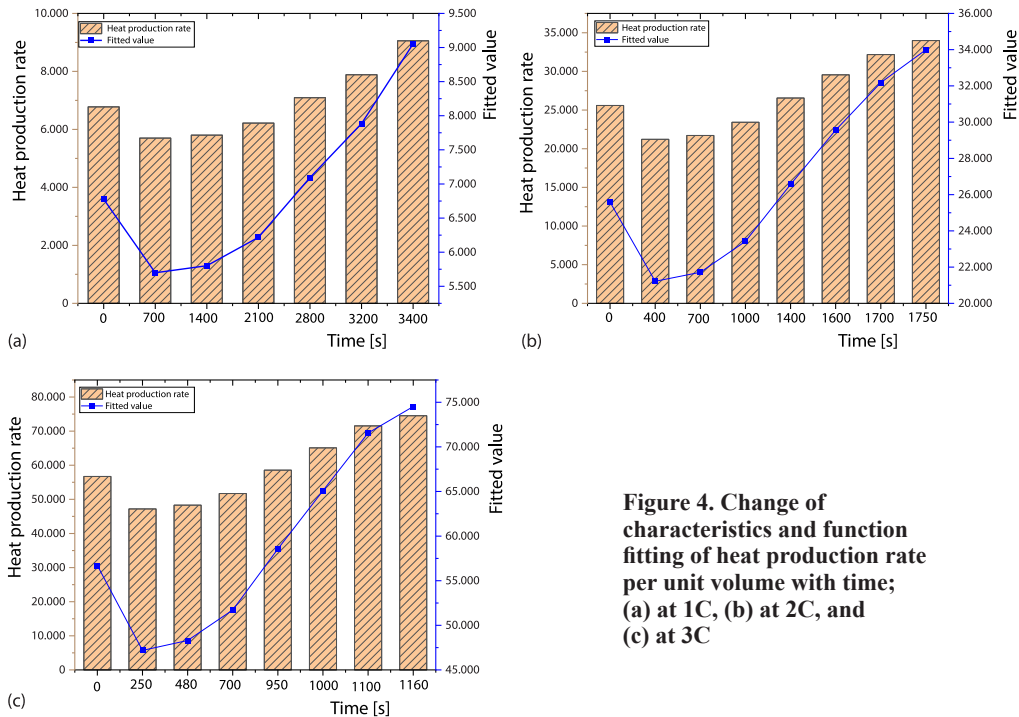
The HPPC method is used to test the change of voltage, current, and the internal resistance which changes with the change of SOC of LiFePO<sub>4</sub>, as shown in fig. 3.

Figure 3 shows the relationship of the current, voltage, and time in the internal resistance test based on HPPC. The test results show that the current of LiFePO<sub>4</sub> batteries changes at the step, and the voltage of the battery gradually decreases during the discharge. The results of internal resistance show that the internal resistance is larger at the initial discharge stage (SOC = 1) and then decreases with SOC.



The heat production of LiFePO<sub>4</sub> batteries during discharge at 1C, 2C, and 3C is shown in fig 4.

The figure shows that the heat production at different discharge rates decreases first and then increases and it also increases with the discharge rate, which is the reason why the temperature rises during discharge.



**Figure 4. Change of characteristics and function fitting of heat production rate per unit volume with time; (a) at 1C, (b) at 2C, and (c) at 3C**

The temperature increase in the experiment and simulation are shown in fig 5.

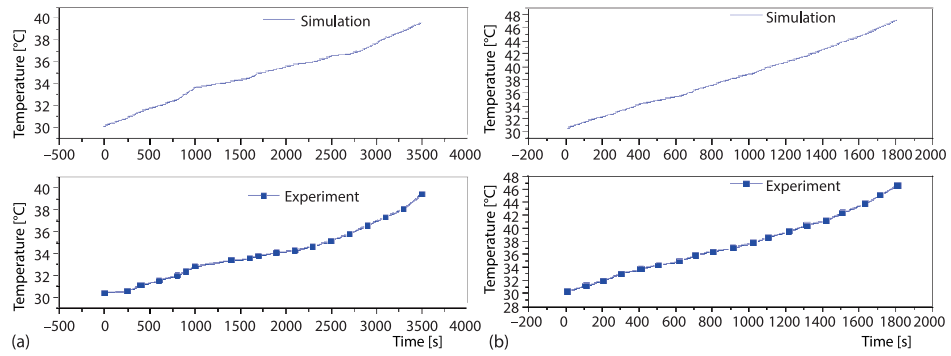
Figure 5 shows the comparison of the highest temperature with time at the discharge rates of 1C, 2C, and 3C in the process of simulation and experiment. The experimental results show that the highest temperature difference at a discharge rate of 1C is 0.5 °C, 0.6 °C at 2C, and 1.2 °C at 3C. The temperature change of the simulation is close to that of the experiment, and the temperature difference is within 1.5 °C, indicating that the numerical simulation results can reflect the temperature change of the battery in the actual discharge.

#### *Results of heat transfer characteristics of lithium battery*

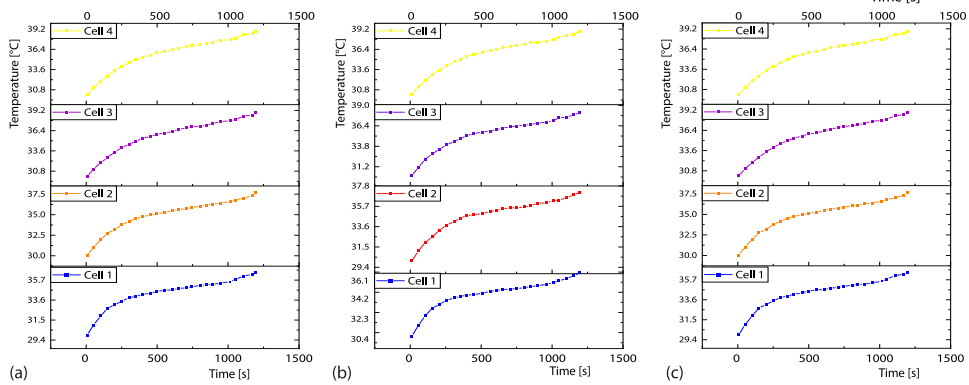
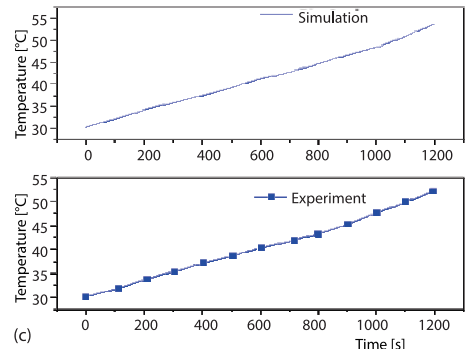
The temperature change with time in different numbers of channels are shown in fig. 6.

Figure 6 shows that the temperature of each battery during discharge changes sharply in the initial and final stages, and increases gently for a long time in the middle stage. The reason is that the heat production is large at the beginning and end of the discharge, which is consistent with the change of the heat production of the aforementioned battery, and the gentle change of the temperature is due to the small heat production and the gradual increase of the temperature difference of the battery and the coolant.

The highest temperature and temperature difference change with time in different numbers of channels are shown in fig. 7.

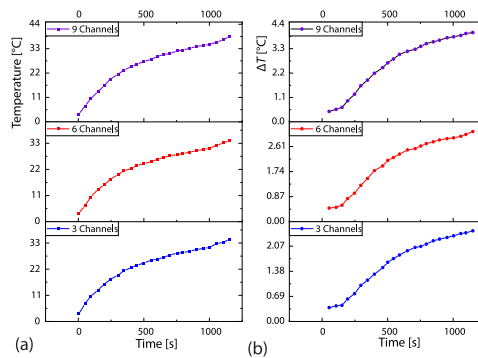


**Figure 5. Experiment and simulation of the temperature rise of the battery; (a) at 1C, (b) at 2C, and (c) at 3C**



**Figure 6. Change of the temperature with time in different number of channels; (a) 3-channel, (b) 6-channel, and (c) 9-channel**

**Figure 7. The highest temperature and temperature difference with time in different numbers of channels; (a) the highest temperature and (b) temperature difference**



The results show that the highest temperatures after discharge are 38.9 °C, 39.1 °C, and 39.8 °C, respectively when 3-, 6-, and 9-channels are used for cooling. When the total mass-flow rate is  $7.2 \cdot 10^{-3}$  kg/s, the three types of channels can control the temperature within 40 °C and achieves the efficiency of temperature control. The 6-channel cold plate has the best effect on temperature control. Figure 7(b) shows that the temperature difference gradually increases with discharge time, and it reaches the maximum at the end of the discharge. After the discharge is completed, the highest temperature difference in the cooling system of 3-, 6-, and 9-channels is 2.1 °C, 2.8 °C, and 4.1 °C, respectively, which tells that the temperature difference control of 3-channel and 6-channel battery pack is better and their temperature differences are within 3 °C.

The highest temperature and temperature difference with time at different mass-flow rates are shown in fig. 8.

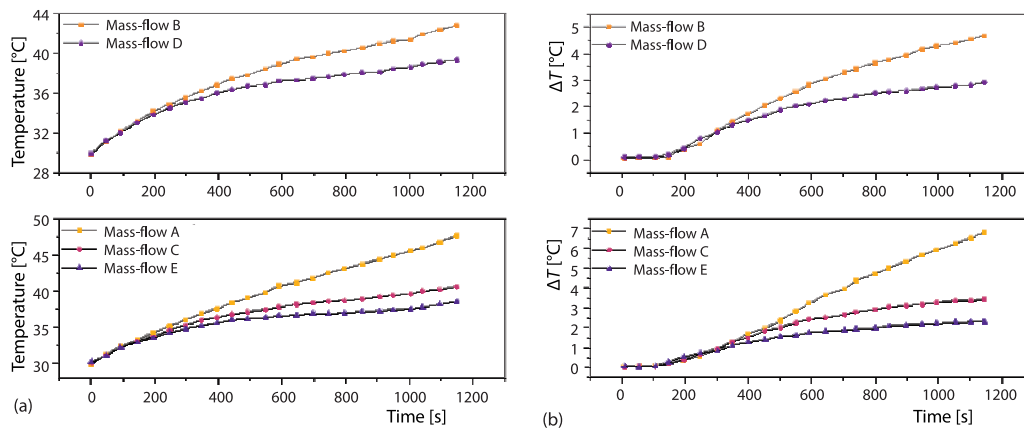


**Figure 8. The highest temperature and temperature difference with time at different mass-flow rates; (a) the highest temperature and (b) temperature difference**

Figure 8 shows the highest temperature and temperature difference with time at 3C discharge rate with 6-channel cold plate at different flow rates. When the total mass-flow rate is 7.2, the battery pack is discharged at  $7.2 \cdot 10^{-3}$  kg/s and the 6-channel cold plate has the best cooling effect on the battery pack. This thermal management method can control the highest temperature below 40 °C and the highest temperature difference within 3 °C during the whole discharge process.

Mass-flow rates affect the highest temperature and temperature difference at different discharge rates is shown in fig. 9.

Figure 9 shows that when liquid cooling is used for thermal management and the battery pack is discharged at 1C and 2C, the requirement for the flow rate of the coolant is low, and the low flow rate can effectively control the temperature. When the battery pack is discharged at a 1C rate, the temperature difference in the battery pack is small, even if the mass-flow rate of coolant is  $1.8 \cdot 10^{-3}$  kg/s, the highest temperature difference is lower than 1.5 °C.

#### *Results of heat transfer characteristics of LiFePO<sub>4</sub> battery based on cooling PCM*

The thermal conductivity and stability control (DSC) of pure PCM and PCM-coupled with expanded graphite are shown in fig. 10.

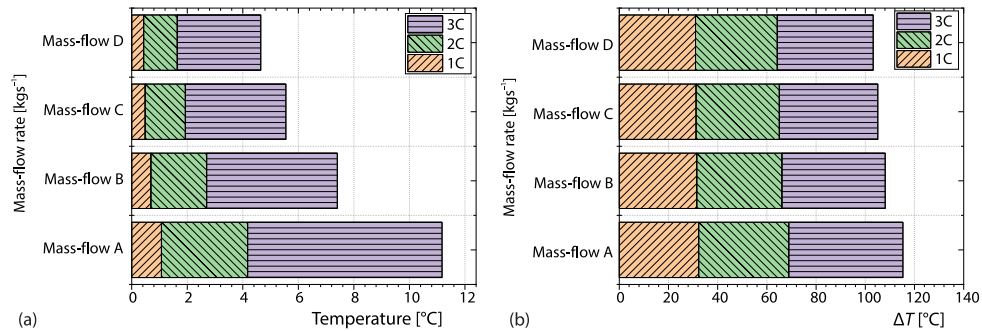


**Figure 9. Influence of mass-flow rate on the highest temperature and temperature difference of the battery at different discharge rates; (a) the highest temperature and (b) temperature difference**

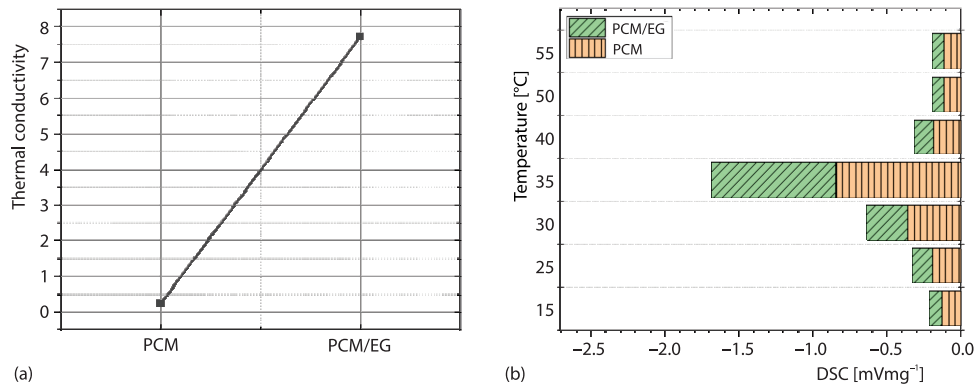


**Figure 10. Thermal conductivity and DSC; (a) thermal conductivity and (b) DSC**

The data show that the thermal conductivity of PCM/EG is 7.51 W/mK, while that of pure paraffin is 0.31 W/mK. The thermal conductivity of the material is increased by 24 times after the pure paraffin is compounded with expanded graphite. This indicates that the expanded graphite has an obvious effect on improving the overall thermal conductivity of the material, and the coupled PCM help to improve the heat absorption rate significantly. Figure 10(b) shows that the latent heat of pure paraffin is 154.96 J/g, while that of coupled PCM of paraffin and expanded graphite is 135.12 J/g. It is concluded that the latent heat of phase change decreases when paraffin and expanded graphite are compounded, and the temperature of coupled PCM is the best working temperature range of LiFePO<sub>4</sub> batteries, meeting the requirements of thermal management.

Under natural-convection, the highest temperature of each cell after discharge at 1C and the highest temperature of the coupled PCM at the discharge rates of 1C, 2C, and 3C are shown in fig. 11.

Figure 11(a) shows the highest temperature of each monomer battery when (natural-convection cooling (ANC) is used after the discharge of the battery pack at 1C discharge rate is completed. The temperature of the third battery is the highest, and the value is 39.9 °C. The temperature of the first battery is the lowest. Figures 11(b) and 11(c) show the increase of the temperature of the third battery after natural-convection cooling and coupling with coupled PCM when the discharge rate is 1C, 2C, and 3C. The results show that the heat management of

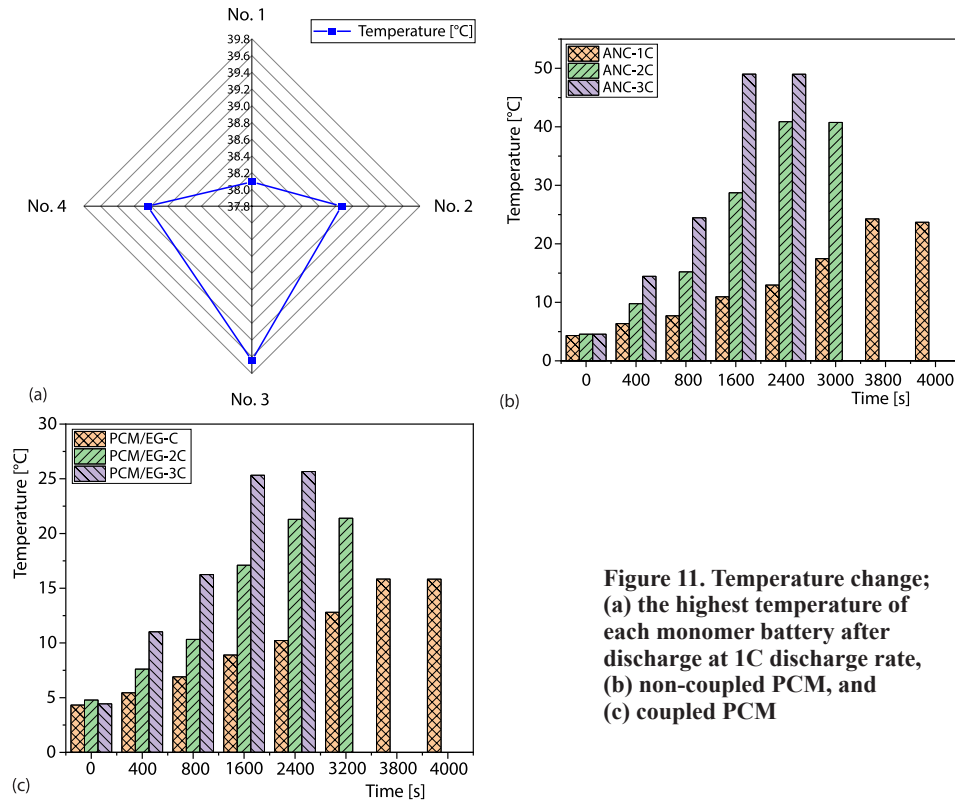


**Figure 11. Temperature change; (a) the highest temperature of each monomer battery after discharge at 1C discharge rate, (b) non-coupled PCM, and (c) coupled PCM**

the battery with PCM can effectively control the temperature of the battery within the optimal operating temperature range required by the battery in a single cycle.

The temperature difference between natural-convection cooling and coupled PCM cooling with time is shown in fig. 12.

Figure 12 shows the temperature difference between natural-convection cooling and coupled PCM cooling with time. The temperature difference of the battery increases with discharge rate, and the temperature difference of cooling PCM is less than that of natural-convection cooling at the same discharge rate.

The results show that the temperature in different cooling channels changes with time in the process of 3C discharge. When the temperature in the 6-channel changes with time ( $T_w = 30\text{ }^\circ\text{C}$ ) and the mass-flow rate is  $2 \cdot 10^{-3}\text{ kg/s}$ , the temperature difference of the battery pack is shown in fig. 13.

Figure 13(a) shows that the cooling time decreases with the increase of the number of channels, and the 6-channel has the best cooling effect. Figure 13(b) shows the change of temperature when the total flow rate is  $1.0 \cdot 10^{-3}\text{ kg/s}$ ,  $2.0 \cdot 10^{-3}\text{ kg/s}$ , and  $3.0 \cdot 10^{-3}\text{ kg/s}$ , in the 6-channel. When the flow rate is  $2.0 \cdot 10^{-3}\text{ kg/s}$ , the highest temperature of the battery during discharge is  $40.1\text{ }^\circ\text{C}$ . The temperature of the battery can be controlled in the optimal operating temperature range. Figure 13(c) shows the temperature difference of the battery pack with the time when 6-channel liquid cooling is used and only PCM are used. The temperature difference decreases after 1178 when the liquid cooling starts. In the whole experiment, the maximum temperature difference of the battery is only  $1.3\text{ }^\circ\text{C}$ , which shows that the heat management of the liquid coupled with PCM cooling can effectively control the temperature of the battery.

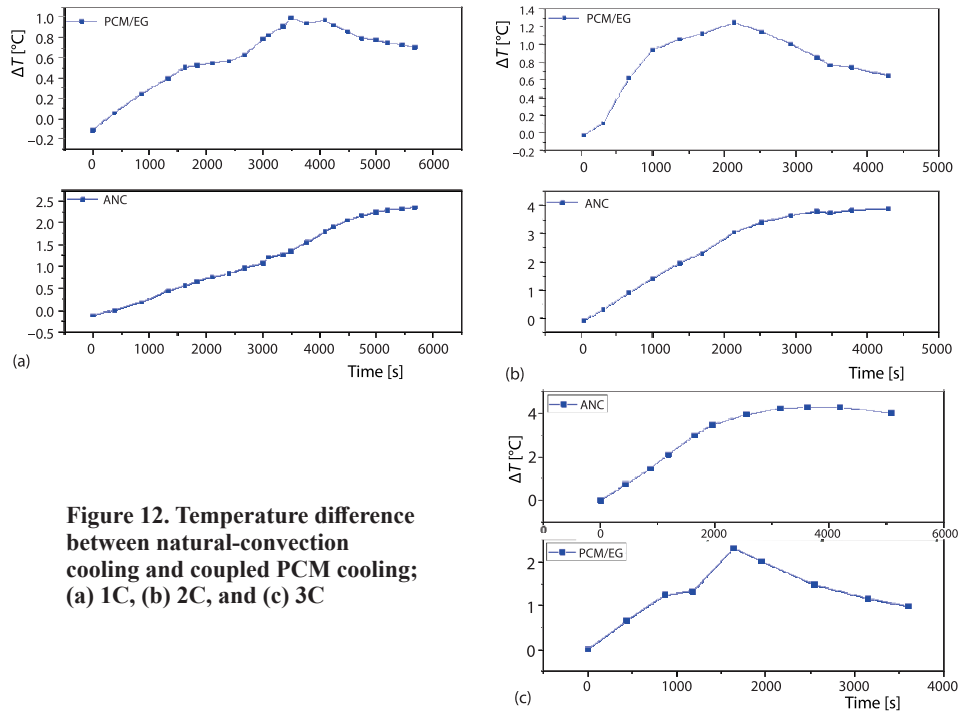


**Figure 12. Temperature difference between natural-convection cooling and coupled PCM cooling; (a) 1C, (b) 2C, and (c) 3C**

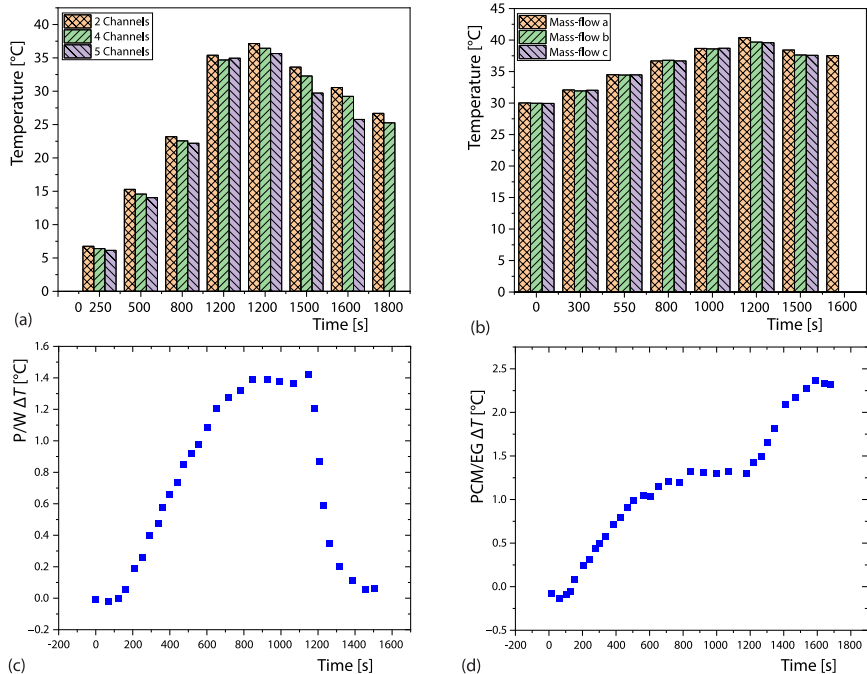


**Figure 13. Temperature and temperature difference with time under different conditions; (a) different channels and mass-flow, (b) different mass-flow in 6-channels, (c) temperature difference with the mass-flow rate of  $2 \cdot 10^{-3}$  kg/s P/W, and (d) temperature difference with the mass-flow rate of  $2 \cdot 10^{-3}$  kg/s PCM/EG**

The change of temperature and temperature difference at 3C charge-discharge rate is shown in fig. 14.

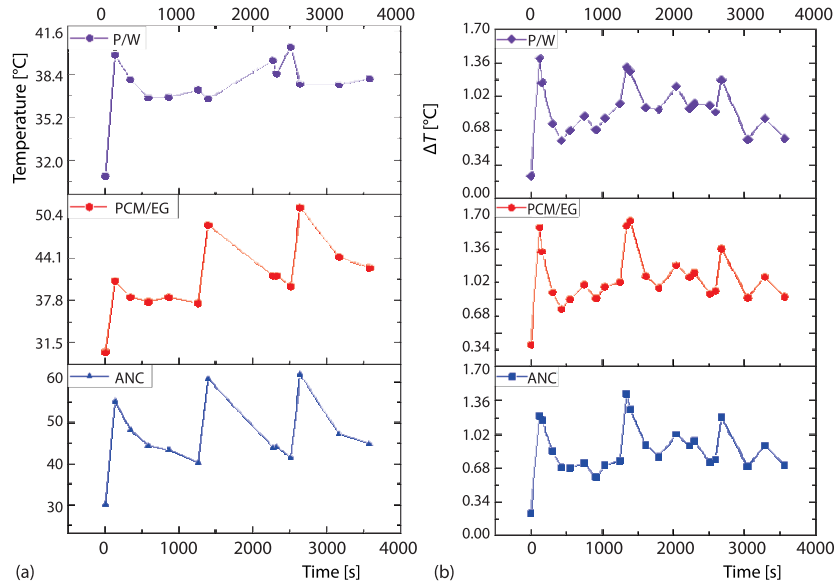


**Figure 14. Change of temperature and temperature difference at 3C charge-discharge rate; (a) temperature change and (b) temperature difference**

Figure 14(a) shows the change of the temperature of the battery at the 3C charge-discharge rate. The PCM can effectively control the temperature of the battery pack during the first cycle. However, as the charging and discharging continue, most of the latent heat of PCM will absorb the heat of the battery. When active liquid cooling is coupled with PCM cooling, the highest temperature of the battery pack can be controlled below 40 °C during the charge and discharge. Figure 14(b) tells that the temperature difference can be controlled below 1.5 °C during the whole cycle. The active liquid cooling coupled with PCM is used for thermal management and has a good effect.

## Conclusion

Power battery is one of the core components of new energy vehicles, and its cycle life and thermal safety are important factors restricting the popularity of new energy vehicles. The heat production of LiFePO<sub>4</sub> batteries is studied to extend the cycle life and prevent the over-heat of the battery. The contribution of the study is that the heat production characteristics of LiFePO<sub>4</sub> batteries are analyzed by simulation analysis and experiments, and the heat transfer characteristics of the thermal management system are studied through liquid cooling, PCM cooling, and coupled channel-PCM cooling. The internal resistance of LiFePO<sub>4</sub> batteries tested by the hybrid pulse method shows that the internal resistance of LiFePO<sub>4</sub> batteries is larger at the beginning and the end of discharge, and the heat production of the battery is also larger at these two-stages. When the mass-flow rate increases, the highest temperature after discharge and the highest temperature difference decrease, but this trend gradually slows down as the mass-flow rate continues to increase.

There are still some shortcomings in this study. When the battery is in a high or low temperature environment, the charge state of the battery is the same, and the terminal voltage

is different. For the same battery and model, how to eliminate the difference at high and low temperatures is a problem that needs to be taken seriously. The LiFePO<sub>4</sub> battery is particularly sensitive to low temperatures, and the actual discharge capacity of the LiFePO<sub>4</sub> battery will be seriously reduced at low temperatures. Therefore, the thermal insulation and heating analysis of LiFePO<sub>4</sub> batteries at low temperatures needs to be further explored. In the follow-up study, the effects of positive and negative materials and the electrolyte of LiFePO<sub>4</sub> battery on the low temperature of the battery will be studied, and the methods to improve the low temperature will be found out.

## References

- [1] Liu, Z., *et al.*, Critical Issues of Energy Efficient and New Energy Vehicles Development in China, *Energy Policy*, 115 (2018), Apr., pp. 92-97
- [2] Vahidi, A., Sciarretta, A., Energy Saving Potentials of Connected and Automated Vehicles, *Transportation Research Part C: Emerging Technologies*, 95 (2018), Oct., pp. 822-843
- [3] Kouchachvili, L., *et al.*, Hybrid Battery-Supercapacitor Energy Storage System for the Electric Vehicles, *Journal of Power Sources*, 374 (2018), Jan., pp. 237-248
- [4] Okada, T., *et al.*, Effect of Environmental Awareness on Purchase Intention and Satisfaction Pertaining to Electric Vehicles in Japan, *Transportation Research – Part D: Transport and Environment*, 67 (2019), Feb., pp. 503-513
- [5] Horn, M., *et al.*, Supercapacitors: A New Source of Power for Electric Cars, *Economic Analysis and Policy*, 61 (2019), Mar., pp. 93-103
- [6] Danielis, R., *et al.*, Probabilistic Total Cost of Ownership Model to Evaluate the Current and Future Prospects of Electric Cars Uptake in Italy, *Energy Policy*, 119 (2018), Aug., pp. 268-281
- [7] An, Z., *et al.*, A Review on Lithium-Ion Power Battery Thermal Management Technologies and Thermal Safety, *Journal of Thermal Science*, 26 (2017), 5, pp. 391-412
- [8] Manthiram, A., A Reflection on Lithium-Ion Battery Cathode Chemistry, *Nature Communications*, 11 (2020), 1, pp. 1-9.
- [9] Zahid, T., *et al.*, State of Charge Estimation for Electric Vehicle Power Battery Using Advanced Machine Learning Algorithm under Diversified Drive Cycles, *Energy*, 162 (2018), Nov., pp. 871-882
- [10] Zhang, X., *et al.*, Experimental Investigation on Thermal Management Performance of Electric Vehicle Power Battery Using Composite Phase Change Material, *Journal of Cleaner Production*, 201 (2018), Nov., pp. 916-924
- [11] Zou, C., *et al.*, A Review of Fractional-Order Techniques Applied to Lithium-Ion Batteries, Lead-Acid Batteries, and Supercapacitors, *Journal of Power Sources*, 390 (2018), June, pp. 286-296
- [12] Lach, J., *et al.*, Applications of Carbon in Lead-Acid Batteries: A Review, *Journal of Solid State Electrochemistry*, 23 (2019), 3, pp. 693-705
- [13] Pan, H., *et al.*, Sustainability Evaluation of Secondary Lead Production from Spent Lead Acid Batteries Recycling, *Resources Conservation and Recycling*, 140 (2019), Jan., pp. 13-22
- [14] Sun, Z., *et al.*, Spent Lead-Acid Battery Recycling in China – A Review and Sustainable Analyses on Mass-Flow of Lead, *Waste Management*, 64 (2017), June, pp. 190-201
- [15] Deyab, M. A., Ionic Liquid as an Electrolyte Additive for High Performance Lead-Acid Batteries, *Journal of Power Sources*, 390 (2018), June, pp. 176-180
- [16] Innocenzi, V., *et al.*, A Review of the Processes and Lab-Scale Techniques for the Treatment of Spent Rechargeable NiMH Batteries, *Journal of Power Sources*, 362 (2017), Sept., pp. 202-218
- [17] Das, V., *et al.*, Recent Advances and Challenges of Fuel Cell Based Power System Architectures and Control – A Review, *Renewable and Sustainable Energy Reviews*, 73 (2017), June, pp. 10-18
- [18] Olabi, A. G., *et al.*, Fuel Cell Application in the Automotive Industry and Future Perspective, *Energy*, 214 (2021), 118955
- [19] Wei, L., *et al.*, Experimental Study on Thermal Management of Cylindrical Li-Ion Battery with Flexible Micro-Channel Plates, *Journal of Thermal Science*, 29 (2020), 4, pp. 1001-1009
- [20] Xie, Y., *et al.*, Experimental and Analytical Study on Heat Generation Characteristics of a Lithium-Ion Power Battery, *International Journal of Heat and Mass Transfer*, 122 (2018), July, pp. 884-894
- [21] Zhou, Z., *et al.*, Quantitative Study on the Thermal Failure Features of Lithium Iron Phosphate Batteries under Varied Heating Powers, *Applied Thermal Engineering*, 185 (2020), 116346

- [22] Cheng, X., *et al.*, Thermal Runaway Characteristics of a Large Format Lithium-Ion Battery Module, *Energies*, 12 (2019), 16, 3099
- [23] Cui, Q., *et al.*, A Stochastic Optimal Energy Management Strategy Considering Battery Health for Hybrid Electric Bus, Proceedings of the Institution of Mechanical Engineers – Part D: *Journal of Automobile Engineering*, 234 (2020), 13, 095440702092428
- [24] Yu, Z., *et al.*, Radially Inwardly Aligned Hierarchical Porous Carbon for Ultra-Long-Life Lithium-Sulfur Batteries, *Angewandte Chemie International Edition*, 59 (2020), 16, pp. 6406-6411
- [25] Yokoshima, T., *et al.*, Direct Observation of Internal State of Thermal Runaway in Lithium Ion Battery during Nail-Penetration Test, *Journal of Power Sources*, 393 (2018), July, pp. 67-74
- [26] Heydarian, A., *et al.*, Application of a Mixed Culture of Adapted Acidophilic Bacteria in Two-Step Bioleaching of Spent Lithium-Ion Laptop Batteries, *Journal of Power Sources*, 378 (2018), Feb., pp. 19-30
- [27] Ciez, R. E., Whitacre, J. F., Examining Different Recycling Processes for Lithium-Ion Batteries, *Nature Sustainability*, 2 (2019), 2, pp. 148-156
- [28] Sheikh, N. A., *et al.*, Comparison and Analysis of the Atangana-Baleanu and Caputo-Fabrizio Fractional Derivatives for Generalized Casson Fluid Model with Heat Generation and Chemical Reaction, *Results in Physics*, 7 (2017), Feb., pp. 789-800
- [29] Fang, Y., *et al.*, Investigation on the Transient Thermal Performance of a Mini-Channel Cold Plate for Battery Thermal Management, *Journal of Thermal Science*, 30 (2021), 5, pp. 914-925